THE SUN AND THE HELIOSPHERE AS AN INTEGRATED SYSTEM

THE SUN AND THE HELIOSPHERE AS AN INTEGRATED SYSTEM

Edited by
GIANNINA POLETTO
INAF, Osservatorio Astrofisico di Arcetri, Firenze, Italy

STEVEN T. SUESS
NSSTC, NASA Marshall Space Flight Center, Huntsville, Alabama, USA

Kluwer Academic Publishers
Boston/Dordrecht/London

A C.I.P. Catalogue record for this book is available from the Library of Congress.

ISBN 1-4020-2830-X (HB)
ISBN 1-4020-2831-8 (e-book)

Published by Kluwer Academic Publishers,
P.O. Box 17, 3300 AA Dordrecht, The Netherlands.

Sold and distributed in North, Central and South America
by Kluwer Academic Publishers,
101 Philip Drive, Norwell, MA 02061, U.S.A.

In all other countries, sold and distributed
by Kluwer Academic Publishers,
P.O. Box 322, 3300 AH Dordrecht, The Netherlands

Contents

Preface xi

1
Hydrogen Walls: Mass Loss of Dwarf Stars and the Young Sun 1
Jeffrey L. Linsky and *Brian E. Wood*
1 Is the Solar Wind Unique? 2
2 Hydrogen Walls: A New Tool for Measuring Mass-Loss Rates 6
2.1 Stellar Astrospheres 12
2.2 The Mass-Loss History of the Sun 17
3 Influence of Stellar Winds on Planets in the Solar System and Beyond 19
4 Conclusions 20

2
The Heliospheric Interface: Models and Observations 23
Vladislav V. Izmodenov
1 Introduction 23
2 Brief Summary of Observational Knowledge 26
2.1 Solar Wind Observations 26
2.2 Interstellar Parameters 27
3 Overview of Theoretical Approaches 29
3.1 H Atoms 30
3.2 Solar Wind and Interstellar Electron and Proton Components 32
3.3 Pickup Ions 34
3.4 Cosmic Rays 34
4 Overview of Heliospheric Interface Models 35
5 Self-Consistent Two-Component Model of the Heliospheric Interface and Recent Advancements of the Model 39
5.1 Plasma 39
5.2 H Atoms 42
5.3 Effects of Interstellar and Solar Wind Ionized Helium 45
5.4 Effects of GCRs, ACRs and the Interstellar Magnetic Field 47
5.5 Effects of the Solar Cycle Variations of the Solar Wind 49
5.6 Heliotail 52
6 Interpretations of Spacecraft Experiments Based on the Heliospheric Interface Model 53
6.1 Pickup ons 54
6.2 Location of the Termination Shock in the Direction of Voyager 1 56

6.3 Filtration of Interstellar Oxygen and Nitrogen 57
7 Summary 57

3
Radiation from the Outer Heliosphere and Beyond 65
Iver H. Cairns
1 Introduction 65
2 Current Observational Status 68
3 Basic Theoretical Issues 73
4 The Priming/GMIR Theory 75
5 Recent Theoretical Results 79
6 Discussion and Conclusions 85

4
Ulysses at Solar Maximum 91
Richard G. Marsden
1 Introduction 91
2 Scientific Highlights at Solar Maximum 93
2.1 Solar Wind 94
2.2 Magnetic Field 99
2.3 Energetic Particles 101
2.4 Cosmic Rays 104
2.5 Interstellar Dust 106
3 The Future of Ulysses 107

5
Propagation of Energetic Particles to High Latitudes 113
T. R. Sanderson
1 Introduction 113
2 Solar Conditions 115
2.1 Influence of the Sun on the Heliosphere 115
2.2 Coronal Magnetic Field During a 22-year Solar Cycle 116
2.3 Coronal Magnetic Field and Coronal Holes During the Ulysses Mission 119
3 The First Orbit 120
4 The Second Orbit 124
4.1 The Second Polar Passes 125
5 Discussion 129
5.1 The Second Northern Polar Pass 129
5.2 Comparison with the Second Southern Polar Pass 138
6 Summary and Conclusions 141

6
Solar Wind Properties from IPS Observations 147
Masayoshi Kojima, Ken-ichi Fujiki, Masaya Hirano, Munetoshi Tokumaru, *Tomoaki Ohmi* and *Kazuyuki Hakamada*
1 Introduction 148
2 Interplanetary Scintillation Measurements 149
2.1 Tomographic Analysis of IPS Observations 150
3 Synoptic Velocity Maps 153
3.1 Solar Cycle Dependence of Solar Wind Velocity Structure 155
4 Correction Factor for CAT Analysis Results 155

5 Coronal Hole Size Dependence of Solar Wind Velocity 158
6 Slow Solar Wind from a Small Coronal Hole 159
7 N-S Asymmetry of High-Latitude Fast Solar Wind 163
8 Velocity Gradient in High-Speed Region 165
9 Bimodal Structure of Solar Wind Velocity 167
10 Summary of Solar Cycle Dependence 170
11 Solar Wind Velocity and Physical Condition in Corona 170
11.1 Data 171
11.2 Cross-Correlation Analysis 172
12 Conclusion 174

7
The Dynamically Coupled Heliosphere 179
Nathan Schwadron
1 Introduction 179
2 Inner Source of Pickup Ions 181
3 Distant Cometary Tails 183
4 Outer Source of Pickup Ions and Anomalous Cosmic Rays 186
5 Ubiquitous Statistical Acceleration 187
6 Magnetic Footpoint Motions Through Speed Transitions and Resulting Particle Acceleration 189
7 FALTS 192
8 Summary 195

8
A Global Picture of CMEs in the Inner Heliosphere 201
N. Gopalswamy
1 Introduction 201
2 Solar Source of CMEs 202
3 CME Morphology 203
4 Physical Properties 206
5 Statistical Properties 207
5.1 CME Speed 208
5.2 CME Acceleration 208
5.3 CME Width 211
5.4 CME Latitude 211
5.5 CME Occurrence Rate 212
5.6 CME Mass and Energy 213
5.7 Halo CMEs 215
6 Associated Activities 218
6.1 Flares and CMEs 219
6.2 Prominence Eruptions 220
6.3 Are There Two types of CMEs? 221
6.4 X-ray Ejecta 221
6.5 CMEs and Radio Bursts 222
6.6 CME Interaction and Radio Emission 225
7 CMEs and Solar Energetic Particles 226
8 CMEs in the Heliosphere 229
8.1 High Latitude CMEs 231
9 CMEs and Solar Polarity Reversal 232
10 CMEs and Cosmic Ray Modulation 233
11 Some Outstanding Questions 236
11.1 CME Initiation 236
11.2 How do CMEs Evolve? 237

12 Summary 240

9
MHD Turbulence in the Heliosphere: Evolution and Intermittency 253
Bruno Bavassano, *Roberto Bruno* and *Vincenzo Carbone*
1 Introduction 254
2 MHD Turbulence Evolution 255
2.1 Ecliptic Turbulence 256
2.2 Polar Turbulence 258
2.3 Conclusions on Turbulence Evolution 263
3 Intermittency 264
3.1 Probability Distribution Functions of Fluctuations and Self–similarity 269
3.2 Radial Evolution of Intermittency 271
3.3 Identifying Intermittent Events 273
3.4 Conclusions on Intermittency 277

10
Waves and Turbulence in the Solar Corona 283
Eckart Marsch
1 Introduction 284
2 Coronal Magnetic Field Structures 284
3 Magnetic Network Activity and Coronal Heating 287
4 Waves and Flows in Loops and Funnels 290
5 Magnetohydrodynamic Waves and Flux Tube Oscillations 293
5.1 Observation and Theory 293
5.2 Oscillations of Thin Flux Tubes 295
5.3 Wave Amplitudes Versus Height from Numerical Models 298
5.4 A Standing Slow Magnetoacoustic Wave 299
6 Plasma Waves and Heating of Particles 301
7 Generation, Transfer and Dissipation of Coronal Turbulence 303
7.1 Generation of Magnetohydrodynamic Waves 303
7.2 Wave Energy Transfer and Turbulent Cascade 304
7.3 Wave Dissipation in the Kinetic Domain 307
7.4 Origin and Generation of Coronal High-Frequency Waves 308
7.5 Ion Velocity Distribution and Wave Absorption 310
8 Summary and Conclusion 313

11
The Influence of the Chromosphere-Corona Coupling on Solar Wind and Heliospheric Parameters 319
Øystein Lie-Svendsen
1 Introduction 320
2 Closed Coronal Loops 322
3 The Modelling Tools 325
4 The Electron-Proton Solar Wind 331
5 Helium in the Corona and Solar Wind 341
6 Summary 349

12
Elemental Abundances in the Solar Corona 353
John C. Raymond

1 Introduction 353
2 Methods 355
2.1 Coronal Observations 355
2.2 Solar Wind Measurements 357
3 FIP Effect 357
Flares 359
Active regions 359
Quiet Sun 360
Coronal Holes 360
Prominences 361
Coronal Mass Ejections 361
Average Coronal FIP Bias 361
Solar Wind 362
4 Gravitational Settling 363
5 Comparison with Other Stars 366
6 Summary 367

13
The Magnetic Field from the Solar Interior to the Heliosphere 373
Sami K. Solanki
1 Introduction 373
2 Solar Interior 374
3 Solar Surface 375
4 Chromosphere and Corona 380
5 The Heliosphere 386
6 Conclusion 389

14
Magnetic Reconnection 397
E. R. Priest and D. I. Pontin
1 Introduction 397
2 Two-Dimensional Reconnection 399
2.1 X-Collapse 399
2.2 Sweet-Parker Reconnection 400
2.3 Stagnation-Point Flow Model 401
2.4 Petschek's Model 402
2.5 More Recent Fast Mechanisms 403
3 Three-Dimensional Reconnection 405
3.1 Structure of a Null Point 405
3.2 Global Topology of Complex Fields 405
3.3 3D Reconnection at a Null Point 407
4 Three-Dimensional Reconnection at an Isolated Non-Ideal Region 408
4.1 Fundamental Properties of 3D Reconnection 409
4.2 Analytical Solutions for 3D Reconnection 410
5 Heating the Solar Corona by Reconnection 412
5.1 Converging Flux Model 413
5.2 Binary Reconnection 413
5.3 Separator Reconnection 414
5.4 Braiding 414
5.5 Coronal Tectonics 415
6 Reconnection in the Magnetosphere 416
6.1 Dayside Reconnection 417
6.2 Nightside Reconnection 418

7 Conclusions 419

Chapter 13

THE MAGNETIC FIELD FROM THE SOLAR INTERIOR TO THE HELIOSPHERE

Sami K. Solanki
*Max-Planck-Institut für Sonnensystemforschung**,
37191 Katlenburg-Lindau, Germany
solanki@linmpi.mpg.de

Abstract The Sun's magnetic field permeates all solar layers from the bottom of the convection zone out to the edge of the heliosphere. Through its continuous interaction with the Sun's flow field, the magnetic field evolves, but also influences these flows. In the solar atmosphere the field also affects the thermal state of the gas, producing such diverse phenomena as dark sunspots in the photosphere, plages in the chromosphere and transition region and x-ray loops in the corona, in addition to a rich collection of dynamic and explosive phenomena. Here a brief overview is given of the magnetic field as it threads it way through all these layers. Emphasis is placed on considering the magnetic field in relation to other quantities from one layer to the other. Results of recent investigations are employed to illustrate the magnetic structure and the processes described here.

Keywords: The Sun: magnetic field - convection zone - photosphere - chromosphere - corona - heliosphere

1. Introduction

The Sun's magnetic field threads its way from the bottom of the convection zone to the edge of the heliosphere. On the way it causes and controls a great variety of phenomena while in turn being plied and

*Previously known as Max-Planck-Institut für Aeronomie

stretched by such processes as convection, differential rotation and the solar wind.

Due to this interaction and the central role played by the magnetic field this review perforce touches upon a large chunk of solar and heliospheric physics. Limited space (to say nothing of the author's laziness) prevents an in-depth coverage of these topics. Instead I'll briefly touch upon a few aspects and refer to other publications for more details. This overview is structured geometrically, moving from deeper or lower solar layers to outer or higher ones. This has a certain logic to it, since the magnetic field is generated in the solar interior, from where it rises to the solar surface and thence spreads into the Sun's atmosphere. There a fraction of the field lines is pulled out into the heliosphere and 'opened' by the solar wind, i.e. stretched until they reach the local interstellar medium.

In almost all cases, it is the lower layers which affect the higher layers. For example, the magnetic field in the photosphere determines to a large extent the magnetic structure of the corona. Consequently, it makes sense to discuss the lower layers first.

2. Solar Interior

The generally accepted idea is that a dynamo located at the base of the convection zone is responsible for the magnetic flux appearing at the solar surface in, e.g., active regions (Schmidt 1993; Ossendrijver 2003). In theoretical studies the dynamo is generally placed in the overshoot layer below the convection zone for stability reasons: it is extremely difficult to store sufficiently large amounts of magnetic flux inside the convection zone without this field becoming unstable to buoyancy (Parker 1975; Schüssler 1979), although Nordlund et al. (1992) have argued that convection, in particular rapid downflows, can pump magnetic flux downwards and store significant amounts of flux in the lower convection zone.

The evidence that the dynamo is located near the convection zone's base is strengthened by recent determinations of the Sun's internal rotation. Such studies, based upon data obtained by the Michelson Doppler Interferometer (MDI; Scherrer et al. 1995) and the Global Oscillations Network (GONG); Harvey et al. 1996), have revealed a strong shear layer between the differentially rotating convection zone and the solidly rotating radiative core (Schou et al. 1992, 1998; Tomczyk et al. 1995; Thompson et al. 2003). The differential rotation deduced from MDI data is plotted in Fig. 1. While the nature, the origin and the location of the helical motions that regenerate the magnetic field are still controversially discussed (Schmitt 1987, 2003; Brandenburg and Schmitt 1998; Dikpati

and Gilman 2001; Parker 1993; Durney 1995), there is increasing support for the idea that the meridional circulation might play an important role in transporting/redistributing the general magnetic flux (Choudhuri et al. 1995; Durney 1995, 1996, 1997; Dikpati and Charbonneau 1999; Nandy and Choudhuri 2001; Küker et al. 2001; Hathaway et al. 2003). There has also been considerable progress in determining the structure and properties of the meridional circulation, seen as a poleward flow of gas at the solar surface (Hathaway 1996; Duvall and Gizon 2000).

The advantage of storing the field in the overshoot layer is that field strengths much stronger than those in equipartition with the kinetic energy of the convection can be built up and stored before the field succumbs to the Parker instability (Ferriz-Mas and Schüssler 1993, 1995).

Such super-equipartion fields are required in order to reproduce various properties of active regions including the correct emergence latitudes, the tilts relative to the East-West direction of the axes connecting the opposite polarities (Joy's law) (Fan et al. 1993, 1994; D'Silva and Choudhuri 1993; Schüssler et al. 1994; Caligarie et al. 1995, 1998).

Not all the magnetic flux that leaves the overshoot layer in the direction of the surface manages to reach it. If the field is too weak it is susceptible to the influences of the convective flows. These can brake the rise of the field and can distort the flux tube (Schüssler 1979). In extreme cases this can even lead to the 'explosion' and destruction of magnetic flux tubes (Rempel and Schüssler 2001).

3. Solar Surface

After the magnetic flux has survived the dangers of a passage through the convection zone, it appears at the solar surface as a bipolar magnetic region. At this stage the magnetic field becomes accessible to direct observation. For example, magnetograms mapping the line-of-sight component of the field or the full magnetic vector can be recorded (an example of a full-disk line-of-sight magnetogram is shown in Fig. 2). A greater amount of information can be obtained from spectropolarimetric observations, which allow more reliable determinations of the magnetic vector (Lites et al. 1994; cf. Landi Degl'Innocenti 1992) and also enable the depth dependence of important atmospheric parameters to be determined (e.g. Solanki 1986; Keller et al. 1990; Ruiz Cobo and Del Toro Iniesta 1992; Frutiger et al. 1990; Westendorp Plaza 1997; Socas Navarro et al. 1999).

The largest and most striking bipolar regions are the active regions appearing in the activity belts. These only form the large-scale end of a broad distribution of sizes of bipolar regions of freshly emerged

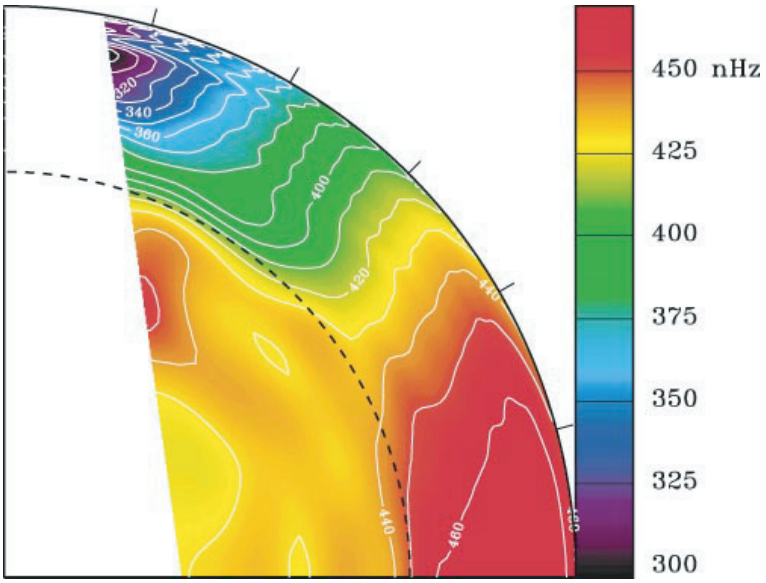

Figure 13.1. Cutaway through the Sun showing rotation frequency (colour coded and iso-frequency contours). The vertical axis is the polar axis, the horizontal axis corresponds to the solar equator, the outer circle (solid) represents the solar surface, the inner circle the bottom of the solar convection zone. The iso-frequency contours running along the convection zone boundary indicate the shear layer (from Thompson et al. 2003, by permission).

flux. Much more common than the active regions are the ephemeral active regions and although each of these individually carries orders of magnitude less flux than an active region, their larger number means that the flux emergence rate in ephemeral regions ($2-4\times10^{26}$Mx/yr) is orders of magnitude larger than in active regions ($3 \times 10^{23} - 3 \times 10^{24}$Mx/yr) (Harvey 1993). This is compensated somewhat by the fact that the lifetime of the flux emerging in the ephemeral regions is 1–2 orders of magnitude shorter (tens of hours; Harvey 1993; Schrijver et al. 1998; Hagenaar et al. 2003) than of active regions (on the order of months).

At the solar surface the magnetic field is filamented into concentrations having sizes ranging from tens of thousands of km (sunspots; for an overview see Thomas and Weiss 1992; Schmieder et al. 1997; Solanki 2003) to below the spatial resolution (magnetic elements; reviewed by Solanki 1993; Stenflo 1994). Although the magnetic field strength averaged over the solar surface is a few tens of Gauss and can vary by large amounts between the quiet Sun and active regions, individual magnetic concentrations often have kG intrinsic field strengths (Hale 1908; Stenflo

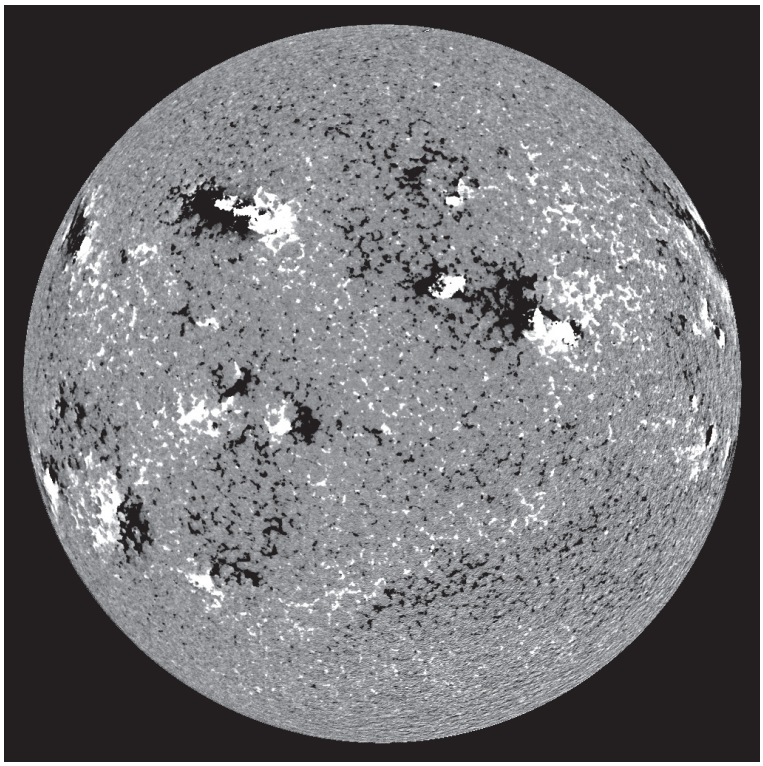

Figure 13.2. Full-disk magnetogram recorded by the Michelson Doppler Interferometer (MDI). Grey areas exhibit little net line-of-sight field, while white and black correspond to opposite polarities. The plotted magnetogram was obtained after integrating over 56 single magnetograms (after compensating for solar rotation) in order to reduce the noise and reveal weaker magnetic features.

1973; Rabin 1992; Rüedi et al. 1992; Solanki 1993). These magnetic concentrations, many of whose global features can be described by simple flux-tube models (e.g. Defouw 1976; Spruit 1976; Deinzer et al. 1984a, b; Jahn and Schmidt 1994; Zayer et al. 1989; Steiner et al. 1986), on closer inspection reveal a highly complex and dynamic (internal) structure. For sunspots this has been deduced directly from observations (e.g., Scharmer et al. 2002; see Sobotka 1997; Solanki 2003 for a review). For the unresolved magnetic elements time series at the highest spatial resolution only give a flavour of the complex internal structure and dynamics (Keller 1992; Berger et al. 1998; Muller et al. 1994). For a more detailed view we have to take recourse to simulations (e.g. Steiner et al.

1998; Gadun et al. 2001; Vögler and Schüssler 2002; Bercik et al. 2003; Vögler 2003).

The latest 3-D simulations of Vögler and co-workers have now reached a level of realism at which they can reproduce sensitive observations with high precision. For example, synthetic G-band images (a spectral region around 430 nm harbouring many CH lines) match the statistical properties and contrasts of observed images after the former have been spatially degraded to the same spatial resolution as the observational data (Schüssler et at. 2003; Shelyag et al. 2004). The comparison is shown in Fig. 3. A detailed analysis reveals that although the temperature at a given height in small magnetic flux concentrations is lower than in the surroundings, they appear brighter (since we observe deeper, hotter layers due to evacuation). Also, it is noticeable that the narrowest magnetic flux sheets are considerably narrower than the intergranular lanes in which they are located (this is visible in both, brightness and velocity maps - the latter not shown in Fig. 3). Thus, almost static gas is co-located with the intense magnetic field, which is bordered on both sides by strong downflows. All these properties are representative of the traditional flux-tube (or flux-sheet; Deinzer et al. 1984a, b) model of magnetic flux concentrations. Other properties predicted by models of thin flux sheets are also seen. These include horizontal pressure equilibrium, the presence of heat influx through the walls and a rapid expansion of the field with height. In addition, the simulations show new features, e.g., in connection with the evolution of magnetic features.

For the largest magnetic structures in the solar photosphere, sunspots, the situation is in some ways reversed. Sunspots are well resolved by observations, which reveal a wealth of detail at all spatial scales. Even the smallest observable scales are important for at least some of the global properties of the sunspot. For example, the complex fine-scale structure of the magnetic and velocity fields in the penumbra (Schmidt et al. 1992; Title et al. 1993; Solanki and Montavon 1993; Westendorp Plaza et al. 1997; Bellot Rubio et al. 2003; Solanki and Rüedi 2003) is responsible for the brightness of the penumbra as a whole (Jahn and Schmidt 1994; Schlichenmaier and Solanki 2003). This makes the self-consistent modelling of sunspots extremely difficult, since a very large range of spatial and temporal scales must be considered simultaneously.

The magnetic field concentrated into sunspots, faculae and the network is also responsible for causing changes in solar irradiance variations. This has been shown convincingly for cycle 23 by Krivova et al. (2003), who employed spectra computed using atmospheric models of these magnetic structures (Unruh et al. 1999) applied to MDI magnetograms in order to reproduce VIRGO (Variability of IRradiance and

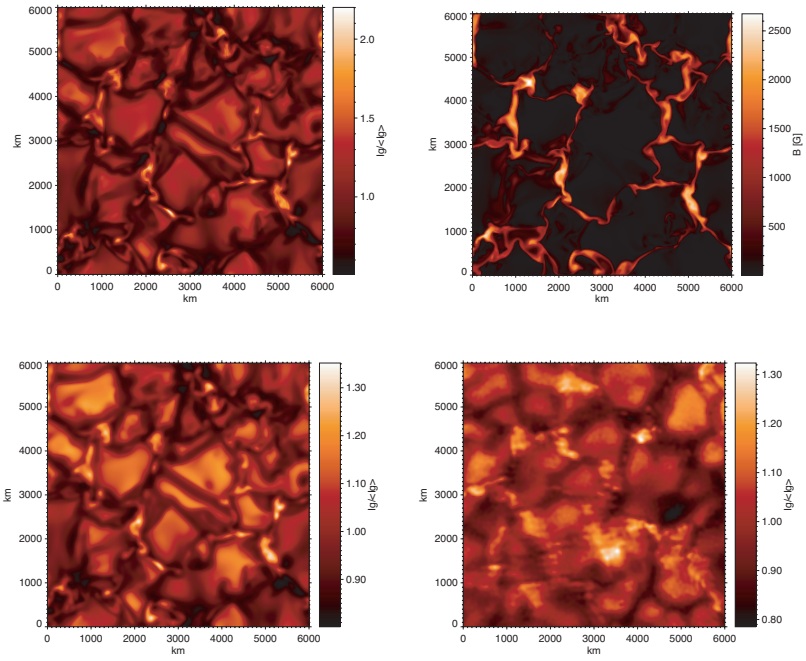

Figure 13.3. Simulated and observed images of the G-band contrast (local G-band brightness divided by spatial average: $I_g/\langle I_g \rangle$) and magnetic structure at the solar surface. Upper left: Synthetic filter image of the simulation area (6000 x 6000 km^2) in the G-band spectral region around 430 nm. The extended bright regions are convective upwellings (granules) surrounded by a network of dark downflow lanes. The small brilliant patches in the dark areas coincide with magnetic flux concentrations. Upper right: Gray shading of the magnetic field strength (in units of Gauss) at the same time step as the G-band contrast image. About two-thirds of the vertical magnetic flux penetrating the simulation box has been assembled into flux concentrations with a field strength above 1000 G (100 mT). Lower left: G-band image after spatial smoothing mimicking the diffraction by a telescope of 1m aperture and the image degradation by the Earth's atmosphere. Lower right: Observed G-band image of the same size as the simulated image with about the same area fraction of G-band bright points as in the simulation (subfield of an image that was taken with the SST on La Palma, courtesy of the Royal Swedish Academy of Sciences). Figure from Schüssler et al. (2003).

Gravity Oscillations; Fröhlich et al. 1995) total and spectral irradiance measurements. They found that on time scales up to the solar cycle, surface magnetic features explain over 90% of the measured total irradiance variations. This conclusion has recently been supported by work done by Livingston and Wallace (2003); Walton et al. (2003) and Woodard and Libbrecht (2003). In particular, the latter authors argue that the con-

clusion reached earlier by Kuhn et al. (1988) that non-magnetic changes are the main cause of irradiance variations over the solar cycle is not tenable.

4. Chromosphere and Corona

The character of the magnetic field changes with height in the atmosphere. The dominating magnetic structures in the photosphere are best described by the flux-tube (or flux sheet) model. This still holds in the lower chromosphere, but the field fans out ever more rapidly with height, finally forming a magnetic canopy, i.e. a layer of almost horizontal field overlying a nearly field-free atmosphere (Giovanelli and Jones 1982; Jones and Giovanelli 1983; Solanki and Steiner 1990). Although it is agreed that the field from different photospheric sources must merge at some height, there is some controversy about the exact value of this height. The situation is also made more complicated by the fact that many of the field lines connect to nearby regions of opposite magnetic polarity, forming low-lying magnetic loops. In any case, in the upper chromosphere the magnetic field is more homogeneous than in the photosphere below. This is clearly borne out by magnetic maps and scans made in He I 10830 Å (Harvey and Hall 1971; Rüedi et al. 1995; Solanki et al. 2003). By the height at which the He I 10830 Å line is formed, near the top of the chromosphere in standard, plane parallel and time independent atmospheric models (Avrett et al. 1994, cf. Fontenla et al. 1993), the magnetic energy density dominates over the thermal energy density almost everywhere. Above that height the structure of the field depends on the distribution in the photosphere of the magnetic flux and of the magnetic field direction (in particular the polarity). In bipolar regions (e.g. active regions) and in mixed polarity regions the dominant structure in the overlying corona is the magnetic loop. If a single magnetic polarity dominates over a sufficiently large area then a large fraction of the field lines are open, i.e. stretched out into the heliosphere by the solar wind. Figure 4 illustrates the general components of the magnetic structure in the solar atmosphere (adapted from Zwaan and Cram 1989). Note that at any given time only a very small fraction (of the order of a few percent) of the Sun's total magnetic flux is in the form of open field, so that the heliospheric field is not necessarily representative of the Sun's total flux. In other words, almost all of the magnetic field lines leaving the Sun's surface, turn around within a few solar radii and return to the solar interior.

Open and closed magnetic flux manifests itself very differently in its respective radiative properties. Almost all of the EUV and X-ray radia-

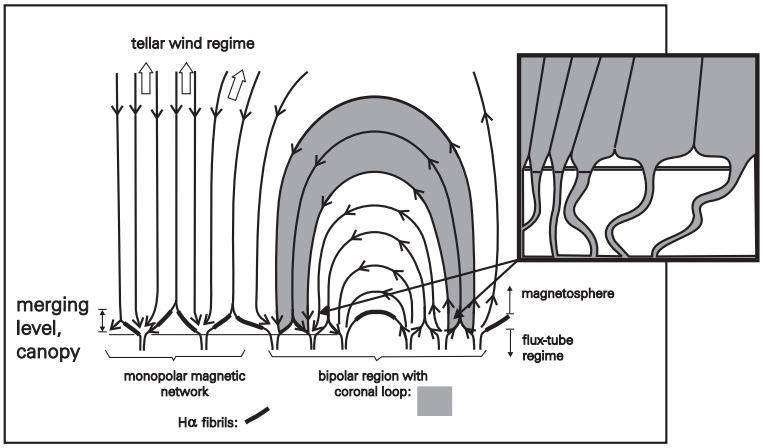

Figure 13.4. Illustration of concepts of the magnetic structure in stellar atmospheres, showing the field rooted in strong flux bundles in the convective zone. The flux-tube domain of discrete flux bundles, separated by nearly field-free plasma, extends upward through the photosphere and into the low chromosphere. In the upper chromosphere the flux tubes merge, creating the magnetic canopy. The magnetosphere, defined as the domain above the merging level, is pervaded by magnetic field. The stellar wind flows along the magnetic field wherever it is (temporarily) open to interstellar space. The inset illustrates that the magnetic field in the photosphere in concentrated in many small fibrils which compose each of the larger elements (e.g. network elements) plotted in the main figure (figure adapted from Zwaan and Cram, 1989).

tion emitted by the Sun comes from closed field lines. I.e., almost all the radiation seen by the SXT instrument on YOHKOH (Acton et al. 1992) and by the channels sampling radiation at above 5×10^5 K in EIT (Delaboudiniére et al. 1995) on SOHO (as well as on TRACE; Handy et al. 1999) comes from closed field regions. A significant fraction of the radiation recorded by the LASCO C2 and C3 coronagraphs (Brückner et al. 1995), however, is emitted by gas located between open field lines. This is mainly due to the relatively large distance to the solar surface sampled by these instruments, since the ratio of open to closed flux increases rapidly with distance from the solar surface. The 'permanently' open field lines, i.e. those remaining open on time scales of multiple weeks or longer, are generally associated with the fast solar wind. In contrast, the slow solar wind is often associated with transiently open magnetic field. The most powerful events during which the field lines open, allowing matter to escape into the heliosphere, are the Coronal Mass Ejections (reviewed e.g., by Webb 2000; Crooker 2000; Gopalswamy et al. 2003).

These different manifestations of closed and open fields are due to a fundamental difference in the way the energy flux input from the solar photosphere (in the form of either wave energy or excess energy in the magnetic field, stored in the form of magnetic tension) is converted into other forms of energy. In a closed field region (i.e. in magnetic loops) no gas can escape across the field lines, so that most of the energy flowing from below is converted into heat and conducted downwards along the field lines, irrespective of the exact mechanism by which the energy is transported and released (wave dissipation, ohmic dissipation of magnetic energy at current sheets or magnetic reconnection; e.g., Narain and Ulmschneider 1996). This hot and dense gas radiates very efficiently.

In open field regions the energy propagating from below is mainly spent accelerating the gas, which then escapes along the field lines in the form of the solar wind. Only a small fraction (estimated to be on the order of 10%) is conducted back down again and radiated away, leading to the fact that coronal holes are much less bright than the quiet Sun (Gabriel 1976).

This simple picture does not explain the fact that at temperatures below approximately 5×10^5 K (e.g. Stucki et al. 2002) coronal holes are equally bright as parts of the quiet Sun containing mainly closed field lines. One proposed solution has been to suggest that many smaller and less hot (transition region) loops are present in both types of regions (Dowdy et al. 1986; Feldman et al. 2000; Feldman 2002; cf. Peter 2002).

The physics of the heating and acceleration processes is complex and, finally, not completely understood. An overview of coronal heating processes is given by Narain and Ulmschneider (1996).

One of the main barriers to progress in this field has been the paucity and limitations of observations of the magnetic field in layers above the solar photosphere. Gyroresonance observations at radio wavelengths have been a major source of our knowledge of the coronal field and have revealed many examples of active regions whose magnetic field is strongly non-potential in the corona (see White 2002 for a review). However, such data (currently) do not have the spatio-temporal resolution needed to resolve the important fine structure. Thus, the structure of magnetic loops has often been derived from either proxy measurements (i.e. brightness structure; Schrijver et al. 1999; Brkovic et al. 2002; Winebarger et al. 2003) or from extrapolations starting from measured photospheric fields (e.g. Lee et al. 1999; Regnier 2002).

Recently, it became possible to deduce the magnetic vector along a set of loops in an emerging flux region. The resulting structure is plotted in Fig. 5 taken from Solanki et al. (2003), cf. Lagg et al. (2003).

At the apex of the highest reconstructed loop, estimated to be roughly 12000–15000 km above the solar surface, the field strength has dropped to roughly 50 G, which is consistent with previous determinations (e.g. from radio observations) of the field strength in coronal loops. These loops are visible in He I 10830 Å because the field along with the gas trapped within it emerged from the solar interior only a short time prior to the observations. Consequently, there had been no time to heat the gas to coronal temperatures. Interestingly, a comparison with extrapolations of field lines starting from the photosphere indicate that the magnetic field was already quite strongly non-potential shortly after emergence. A potential field extrapolation results in a very poor correspondence with the observations, while a constant-α force-free field reproduces the observations already much better (Wiegelmann et al. in preparation). Consequently, significant currents were already present shortly after emergence and must have been built up in the solar interior during the passage of the emerged loop through the convection zone.

Currents are continually fed and supported also later in the life of an active region. It was proposed by Parker (1983, 1988) that the photospheric footpoints of magnetic field lines are continuously shuffled around by convective motions. He argued that these motions lead to the formation of tangential discontinuities or electric current sheets in the corona where energy is dissipated. Strong support for this mechanism as a major heating process in the corona is provided by the work of Gudiksen and Nordlund (2002). Taking a photospheric magnetogram and the potential field extrapolated from it as a starting point, they randomly moved the photospheric magnetic features around with a velocity field exhibiting roughly the horizontal convective velocity spectrum. They then computed the temporal evolution of the resulting coronal magnetic structure, finding that current sheets are continuously being formed, where magnetic energy is dissipated, heating the coronal gas to over a million degrees, with a considerable distribution of temperatures. Interestingly, the picture they obtain for the gas in a limited temperature range (illustrative of the 171 Å channel of TRACE, the Transition Region and Coronal Explorer (Handy et al. 1999)), is much more intermittent and filamented than the magnetic field, in good agreement with the images returned by TRACE in this channel (Schrijver at al. 1999).

Further support for a heating mechanism involving Ohmic dissipation or reconnection at a current sheet comes from the detection of a current sheet using He I 10830 Å spectropolarimetry. This is the first direct detection of an electric current sheet in a layer of the solar atmosphere relevant for coronal and chromospheric heating. The difficulty in mea-

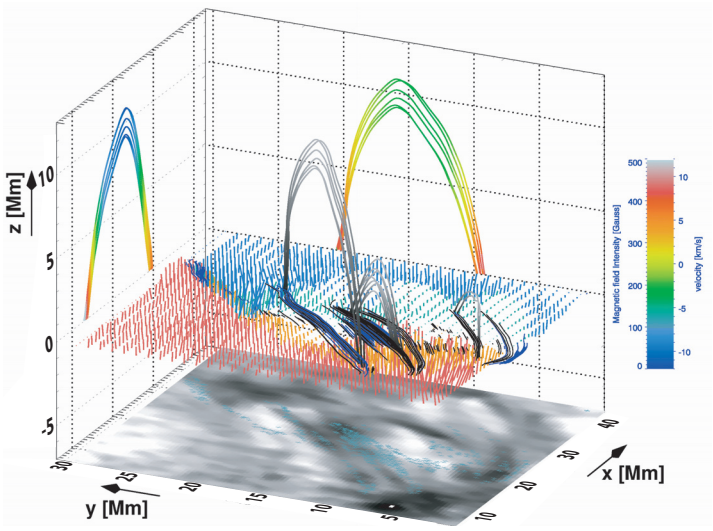

Figure 13.5. Reconstructed magnetic loops in an emerging flux region. The map of the He I 10830 Å lines equivalent width at the bottom is overlaid by a magnetic polarity and connectivity map over which examples of reconstructed loops are plotted. The derived azimuth and inclination angles of the magnetic field in each of the map's pixels are used to trace magnetic field lines. Heavy black lines are projections onto a fixed height of loops that could be successfully reconstructed. These loops trace the equivalent width pattern (shown at the bottom of the plot). Some representative loop field lines are also plotted and for one of the plotted loops they are projected onto the xz- and yz-planes. The color-coding of the loop projections represents the line-of-sight (i.e. basically vertical) velocity (yz-plane) and the magnetic field strength (xz-plane). The loops are rooted in areas with downflowing material, while in the apex upflowing material is observed. This observation, combined with the frozen-in horizontal magnetic field implies that the whole loop is rising. The magnetic field strength decreases with height in both legs from about 390 and 500 Gauss at the two chromospheric footpoints to below 50 Gauss at the apex. Magnetic field vectors at the footpoints of the field lines are shown to visualize the overall magnetic field geometry and strength. Field lines out of (into) the plane parallel to the solar surface are coded in red and orange (blue and green), with orange and green marking field lines for which both footpoints lie within the observed area and emission is seen from the whole length of the loop (see Solanki et al. 2003).

suring such a current sheet lies in the necessity to map the full magnetic vector at chromospheric or coronal heights. Over a distance corresponding to the spatial resolution element of the observations the magnetic vector changes sign within a region of emerging flux in a young active region. This feature is illustrated in Fig. 6, where the current sheet is the narrow valley in the field strength. At the height at which the He I

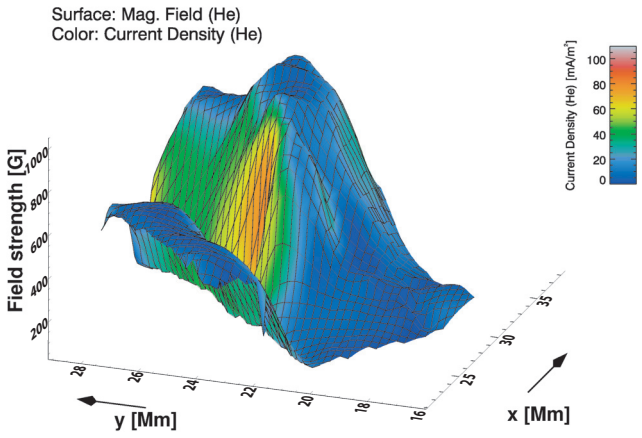

Figure 13.6. Representation of an electric current sheet near the base of the corona. The elevation of the meshed surface is proportional to the magnetic field strength in the upper chromosphere, as derived from the He I 1083 nm line. A narrow valley of low magnetic field values separates two areas of opposite magnetic polarity, so that an electric current flows along this boundary parallel to the Solar surface. The color-coding in the figure indicates the current density of this current sheet calculated using Ampére's Law. The maximum value of approximately 90 mA/m^2 in the region of the largest magnetic field gradient perpendicular to the current sheet represents only a lower limit of the actual current flowing in this chromospheric current sheet. The width of the valley in the magnetic field strength corresponds to the spatial resolution of 1 Mm, limited by turbulence in the Earth's atmosphere, so that the horizontal gradient of the magnetic field is underestimated (see Solanki et al. 2003).

10830 Å line is formed the field is far more homogeneous in strength than in the photosphere with a magnetic filling factor very close to unity (see description given earlier in this section; cf. Harvey and Hall 1971; Rüedi et al. 1995; Penn and Kuhn 1995). Therefore the gradient between the opposite magnetic polarities is expected to be significantly larger than deduced from the observations (since horizontal gradients are reduced by seeing). Hence the obtained current density, up to 90 mA/m^2 is probably a lower limit. Unfortunately, neither TRACE, EIT, YOHKOH nor BBSO Hα images or movies were available for the day, of these observations, so that it cannot be checked whether this current sheet was responsible for any flare-like episodes.

5. The Heliosphere

The heliospheric magnetic field is characterized by the fact that higher order multipoles, needed to describe the field at the solar surface, have decayed away beyond a distance of a few solar radii, so that the dipole component dominates the structure. In addition, beyond the Alfvén radius the energy density of the gas (in particular the kinetic energy density of the solar wind) is far larger than the magnetic energy density (e.g. Weber and Davis 1967). Thus the situation there is reversed relative to the corona. Consequently, the magnetic field is more or less passively dragged along by the solar wind. Logically, only open field lines are present in the heliosphere, if we exclude the magnetic field associated with CMEs and other transient events, which may for some time still be anchored in the photosphere. Due to the combination of the Sun's rotation and the outward motion of the gas the magnetic field follows a spiral pattern (see below).

In recent years very significant progress regarding our knowledge of heliospheric fields has come from the Ulysses spacecraft, which allowed the first measurement of the field outside the ecliptic. The magnetic field strength and solar wind speed during the first Ulysses orbit, carried out under quiet-Sun conditions, is plotted vs. time in Fig. 7, with the heliographic latitude indicated in the top frame (from Balogh and Forsyth 1998). Clearly, at high northern and southern latitudes the field is homogeneous in strength. Although not plotted here, the direction of the magnetic field is also homogeneous at high latitudes, with the azimuth being opposite in both hemispheres, corresponding to opposite magnetic polarities. Note that the gradual increase of the field strength towards the equator in 1994 and 1995 is mainly due to the decreasing distance of the spacecraft to the Sun. This relatively homogeneous field is mainly anchored in the polar coronal holes.

Closer to the ecliptic the field becomes inhomogeneous in both strength and direction, exhibiting multiple jumps of around 180° in azimuth. The magnetic field strength exhibits spikes over which the strength varies by a factor of up to four.

A simple but quite successful model of the large-scale structure of the coronal magnetic field at activity minimum is due to Banaszkiewicz et al. (1998), cf. Forsyth and Marsch (1999). It is composed of dipolar, quadrupolar and equatorial current sheet components. Fig. 8 shows the resulting magnetic structure. Overplotting this on a coronagraphic LASCO C1 brightness image obtained at solar activity minimum exhibits a good agreement (Forsyth and Marsch 1999). According to current thinking the jumps in the magnetic field direction seen by Ulysses

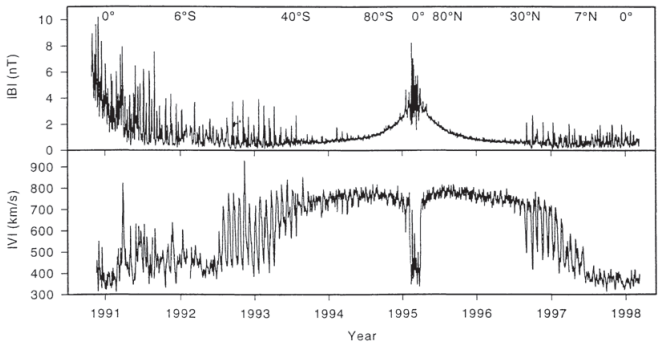

Figure 13.7. The magnitude of the magnetic field and the velocity of the solar wind measured by Ulysses from the beginning of the mission in October 1990 to early March 1998. The heliographic latitude of Ulysses at selected times are indicated in the top frame (figure from Balogh and Forsyth 1998, by permission).

are produced when the spacecraft passes through the current sheet at the equator. This current sheet is warped (appearing like a ballerina's skirt; Schwenn 1990, 1993). Since the Sun completes multiple rotations during the time that the spacecraft crosses the equatorial belt, i.e. the range of latitudes over which the current sheet is warped, the spacecraft can pass through the current sheet multiple times during its passage from pole to pole.

The forces exerted by the solar wind on the field attempt to make it radial, in the absence of solar rotation. When combined with solar rotation, acting through the photospheric footpoints of the field, (which are frozen into the gas) a spiral structure of the field is produced in the equatorial plane (called the Parker spiral; Parker 1958), while outside this plane the field lines follow spirals along cones, with the cones becoming increasingly narrower toward the poles.

Parker's picture has been extended by Fisk (1996) to include the effect of a misalignment between the Sun's axis of rotation and its magnetic dipole axis, as well as of the motion of the magnetic footpoints on the solar surface due to differential rotation (compared to a fixed rotation of the coronal field). This leads to a stronger and less regular displacement of the field lines, in particular at larger distances from the Sun.

Finally, I would like to present an example where the magnetic field at the solar surface directly influences measurements made in the heliosphere by the SWICS instrument (Gloeckler et al. 1992) on Ulysses. In the top panel of Fig. 9 the heliospheric latitude of the Ulysses spacecraft and the sunspot number (as a measure of solar activity) are plotted vs.

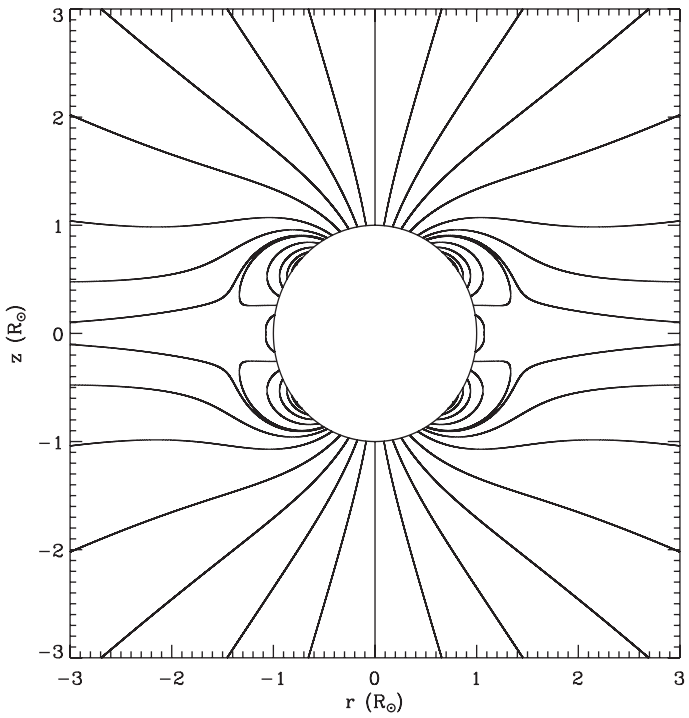

Figure 13.8. The magnetic field lines for the Dipole-Quadrupole-Current-Sheet model of Banaszkiewicz et al. (1998) out to 3 solar radii (solid curves). The model reproduces various observational constraints from SOHO and Ulysses (figure kindly provided by N.-E. Raouafi).

time. In the next panel the solar wind speed and the O^{+7}/O^{+6} abundance ratio measured by SWICS on Ulysses are plotted. It is evident that whereas the solar wind speed is nearly the same while Ulysses is above the southern and the northern coronal holes (marked by the two sets of vertical, dotted lines) the O^{+7}/O^{+6} ratio is significantly different. This ratio is a measure of coronal temperature, so that the southern polar coronal hole (sampled in 1994) was 10–15 % hotter than the northern polar coronal hole in 1995. In the bottom panel of Fig. 9 the spatially averaged field strength at the solar surface in the southern (open circles) and northern polar coronal holes is plotted. It is obvious that the average field strength is higher under the southern polar coronal hole (which is also hotter). This suggests that the average photospheric field strength is closely related to the coronal temperature in coronal holes and the relative abundance of ions in the heliosphere (Zhang et al. 2002).

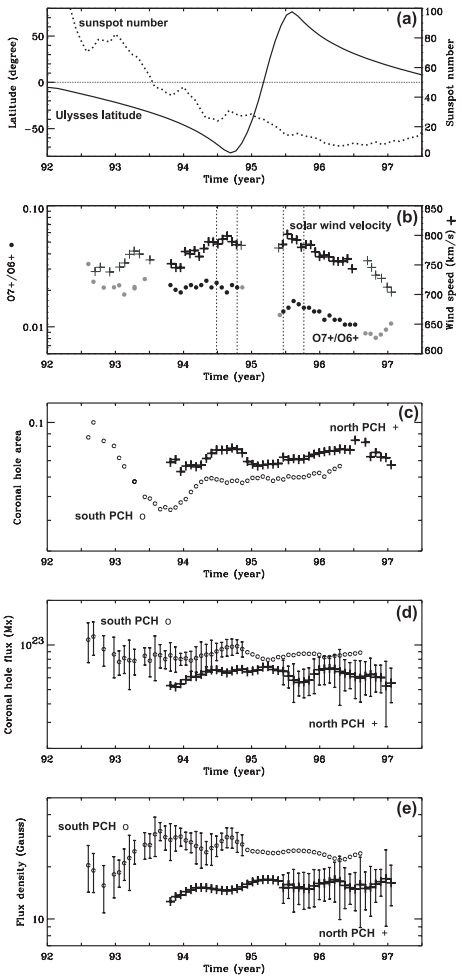

Figure 13.9 Selected solar wind and polar coronal hole parameters between 1992 and 1997. (a) Heliographic latitude of Ulysses and sunspot number; (b) O^{7+}/O^{6+} ratio and solar wind speed as measured by SWICS/Ulysses from 1992 to 1997 (heavy symbols denote pure PCH stream observations, light symbols observations from the mid-latitude fast-slow wind interface regions); (c) area of the south PCH (o) and north PCH (+) estimated from Kitt Peak He I 1083 nm synoptic maps as fraction of the solar surface; (d) magnetic flux of the south (north) PCH derived from Kitt Peak synoptic maps, error bars are included for the south (north) PCH values over the south (north) Ulysses PCH stream intervals; (e) same as in (d) but for magnetic flux density (from Zhang et al. 2002).

6. Conclusion

The magnetic field and its interaction with the solar plasma passes through a variety of regimes from the solar convection zone to the heliosphere. In some layers the magnetic energy density far exceeds the kinetic or thermal energy density, in others it is the opposite, while in yet others the values are similar. The structure and dynamics of the field also change very strongly between convection zone and heliosphere. This variety is one cause of the richness of the types of solar phenomena caused by the magnetic field. More details can be found in the volume edited by Sawaya-Lacoste (2002) as well as the monographs by Parker (1979), Priest (1982), Stenflo (1994) and Zwaan and Schrijver (2000).

Acknowledgements: D. Schmitt critically read through a part of the paper and provided many references. E. Marsch, N.-E. Raouafi, M. Schüssler, A. Vögler and J. Woch provided material and references. My sincere thanks go to all of them.

References

Acton L., Tsuneta S., Ogawara Y., et al., 1992, *Science* **258**, 618.

Avrett E.H., Fontenla J.M., Loeser R., 1994, in *Infrared Solar Physics*, IAU Symp. No. 154, D.M. Rabin et al. (Eds.), Kluwer, Dordrecht, p. 35.

Balogh A. and Forsyth R.J., 1998, The results of the Ulysses mission: A survey of the Heliosphere in three dimensions. In: *Crossroads for European Solan and Heliospheric Physics: Recent Achievements and Future Mission Possibilities*, R.A. Harris (Ed.), ESA SP-417, p. 45.

Banaszkiewicz M., Axford W.I., McKenzie J.F., 1998, *Astron. Astrophys.* **337**, 940.

Bellot Rubio L.R., Balthasar H., Collados M., Schlichenmaier R., 2003, *Astron. Astrophys.* **403**, L47.

Bercik D.J., Nordlund Å., Stein R.F., 2003, Magnetoconvection and micropores. In: *SOHO 12/GONG+ 2002. Local and global helioseismology: the present and future*, H. Sawaya-Lacoste (Ed.), ESA SP-517, p. 201.

Berger T.E., Löfdahl M.G., Shine R.S., Title A.M., 1998, *Astrophys. J.* **495**, 973.

Brandenburg A., and Schmitt D., 1998, *Astron. Astrophys.* **338**, L55.

Brkovic A., Landi E., Landini M., Rüedi I., Solanki S.K., 2002, *Astron. Astrophys.* **383**, 661.

Brueckner G.E., Howard R.A., Koomen M.J. et al., 1995, *Sol. Phys.* **162**, 357.

Caligari P., Moreno-Insertis F., and Schüssler M., 1995, *Astrophys. J.* **411**, 886.

Caligari P., Schüssler M., and Moreno-Insertis F., 1998, *Astrophys. J.* **502**, 481.

Choudhuri A.R., Schüssler M., and Dikpati M., 1995, *Astron. Astrophys.* **303**, L29.

Crooker, N., 2000, *J. Atmosph. Solar Terr. Phys.* **62**, 1071.

Defouw R.J., 1976, *Astrophys. J.* **209**, 266.

Deinzer W., Hensler G., Schüssler M., Weisshaar E., 1984a, *Astron. Astrophys.* **139**, 426.

Deinzer W., Hensler G., Schüssler M., Weisshaar E., 1984b, *Astron. Astrophys.* **139**, 435.

Delaboudiniére J.-P., Artzner G.E., Brunaud J. et al., 1995, *Sol. Phys.* **162**, 291.
Dikpati M., and Charbonneau P., 1999, *Astophys. J.* **518**, 508.
Dikpati M., and Gilman P.A., 2001, *Astophys. J.* **559**, 428.
Dowdy J.F. Jr., Rabin D., Moore R.L., 1986, *Sol. Phys.* **105**, 35.
D'Silva S., Choudhuri A.R., 1993, *Astron. Astrophys.* **272**, 621.
Durney B.R., 1995, *Sol. Phys.* **160**, 213.
Durney B.R., 1996, *Sol. Phys.* **166**, 213.
Durney B.R., 1997, *Astrophys. J.* **486**, 1065.
Duvall T.L., Jr., Gizon L., 2000, *Sol. Phys.* **192**, 177.
Fan Y., Fisher G.H., and Deluca E.E., 1993, *Astrophys. J.* **405**, 390.
Fan Y., Fisher G.H., and Deluca E.E., 1994, *Astrophys. J.* **436**, 907.
Feldman U., 2002, In: *From Solar Min to Max: Half a Solar Cycle with SOHO. Proc. SOHO11 Symp.*, A. Wilson (Ed.), ESA SP-508, p. 531.
Feldman U., Dammasch I., Wilhelm K., 2000, *Space Sci. Rev.* **93**, 411.
Ferriz-Mas A. and Schüssler M., 1993, *Geophys. Astrophys. Fluid Dyn.* **72**, 209.
Ferriz-Mas A. and Schüssler M., 1995, *Geophys. Astrophys. Fluid Dyn.* **81**, 233.
Fisk L., 1996, *J. Geophys. Res.* **101**, 15547.
Fontenla J.M., Avrett E.H., Loeser R., 1993, *Astrophys. J.* **406**, 319.
Forsyth R.J. and Marsch E., 1999, *Space Sci. Rev.* **89**, 7.
Fröhlich C., Romero J., Roth H., et al., 1995, *Sol. Phys.* **162**, 10.
Frutiger C., Solanki S.K., Fligge M., Bruls J.H.M.J., 2000, *Astron. Astrophys.* **358**, 1109.
Gabriel A. H., 1976, *Phil. Trans. Royal Society, Ser. A* **281**, 339.
Gadun A.S., Solanki S.K., Sheminova V.A., Ploner S.R.O., 2001, *Sol. Phys.* **203**, 1.
Giovanelli R.G. and Jones H.P., 1982, *Sol. Phys.* **79**, 267.
Gloeckler et al., 1992, *Astron. Astrophys. Suppl. Ser.* **92**, 267.
Gopalswamy N., Lara A., Yashiro S., Nunes S., Howard R.A., 2003, Coronal mass ejection activity during solar cycle 23. In: *Proc. ISCS 2003 Symposium: Solar Variability as an Input to the Earth's Environment*, ESA-SP-535, p. 403.
Gudiksen B.V. and Nordlund R., 2002, *Astrophys. J.* **572**, 113.
Hagenaar H.J., Schrijver C.J., Title A.M., 2003, *Astrophys. J.* **584**, 1107.
Hale G.E., 1908, *Astrophys. J.* **28**, 315.
Handy B.N., Acton L.W., Kankelborg C.C., et al., 1999, *Sol. Phys.* **187**, 229.
Harvey K.L., 1993, PhD Thesis, Rijksuniv. Utrecht.
Harvey J.W. and Hall D.N.B., 1971, in *Solar Magnetic Fields*, R. Howard (Ed.), IAU Symp. 43, Reidel, Dordrecht, p. 279.

Harvey J.W., Hill F., Hubbard R., et al., 1996, *Science* **272**, 1284.
Hathaway D.H., 1996, *Astrophys. J.* **460**, 1027.
Hathaway D.H., Nandy D., Wilson R.M., Reichmann E.J., 2003, *Astrophys. J.* **589**, 665.
Jahn K. and Schmidt H.U., 1994, *Astron. Astrophys.* **290**, 295.
Jones H.P., Giovanelli R.G., 1983, *Sol. Phys.* **87**, 37.
Keller C.U., 1992, *Nature* **359**, 307.
Keller C.U., Steiner O., Stenflo J.O., Solanki S.K., 1990, *Astron. Astrophys.,* **233**, 583.
Krivova N.A., Solanki S.K., Fligge M., Unruh Y.C., 2003, *Astron. Astrophys.* **399**, L1.
Kuhn J.R., Libbrecht K.G., Dicke R.H., 1989, *Science* **242**, 908.
Küker M., Rüdiger G., and Schultz M., 2001, *Astron. Astrophys.* **374**, 301.
Lagg A., Woch J., Krupp N., Solanki S.K., 2003, *Astron. Astrophys.* in press.
Landi Degl'Innocenti E., 1992, In: *Solar Observations: Techniques and Interpretation*, F. Sánchez, M. Collados, M. Vázquez (Eds.), p. 71.
Lee J., White S.M., Kundu M.R., Mikic Z., McClymont A.N., 1999, *Astrophys. J.* **510**, 413.
Lites B.W., Martínez Pillet V., Skumanich A., 1994, *Sol. Phys.* **155**, 1.
Livingston W., L. Wallace L., 2003, *Sol. Phys.* **212**, 227.
Muller R., Roudhier Th., Vigneau J., Auffret H. 1994, *Astron. Astrophys.* **283**, 232.
Nandy D., and Choudhuri A.R., 2001, *Astrophys. J.* **551**, 576.
Narain U. and Ulmschneider P., 1996, *Space Sci. Rev.* **75**, 453.
Nordlund Å., Brandenburg A., Jennings R.L., et al., 1992, *Astrophys. J.* **392**, 647.
Ossendrijver M., 2003, *Astron. Astrophys. Rev.* **11**, 287.
Parker E.N., 1958, *Astrophys. J.* **128**, 664.
Parker E.N., 1975, *Astrophys. J.* **198**, 205.
Parker E.N., 1979, *Cosmical Magnetic Fields: Their Origin and their Activity*, Clarendon Press, Oxford.
Parker E.N., 1983, *Astrophys. J.* **264**, 642.
Parker E.N., 1988, *Astrophys. J.* **330**, 474.
Parker E.N., 1993, *Astrophys. J.* **408**, 707.
Penn M.J. and Kuhn J.R., 1995, *Astrophys. J.* **441**, 51.
Peter H., 2002, In: *Proc. SOHO 11 Symp., From Solar Min to Max: Half a Solar Cycle with SOHO*, A. Wilson (Ed.), ESA SP-508, p. 237.
Priest E.R., 1982, *Solar Magnetohydrodynamics*, Reidel Publ. Co., Dordrecht.
Rabin D., 1992a, *Astrophys. J.* **390**, L103.

Rabin D., 1992b, *Astrophys. J.* **391**, 832.
Régnier S., Amari T., Kersalé E., 2002, *Astrophys. J.* **392**, 1119.
Rempel M. and Schüssler M., 2001, *Astrophys. J.* **552**, L171.
Rüedi I., Solanki S.K., Livingston W., Stenflo J.O., 1992, *Astron. Astrophys.* **263**, 323.
Rüedi I., Solanki S.K., Livingston W.C., 1995, *Astron. Astrophys.* **293**, 252.
Ruiz Cobo B., Del Toro Iniesta J.C., 1992, *Astrophys. J.* **398**, 375.
Sawaya-Lacoste H. (Ed.), 2002, *SOLMAG 2002: Proc. Magnetic Coupling of the Solar Atmosphere*, Euroconference and IAU Colloquium 188, ESA SP-505.
Scharmer G.B., Gudiksen B.V., Kiselman D., Löfdahl M.G., Rouppe van der Voort L.H.M., 2002, *Nature* **420**, 151.
Scherrer P.H., Bogart R.S., Bush R.I., et al., 1995, *Sol. Phys.* **162**, 129.
Schlichenmaier R. and Solanki S.K., 2003, *Astron. Astrophys.* **411**, 257.
Schmidt D., 1987, *Astron. Astrophys.* **174**, 281.
Schmidt D., 1993, The solar dynamo. In: *IAU Symp. 157: The Cosmic Dynamo*, F. Krause, K.H. Rädler, G. Rüdiger (Eds.), Kluwer, Dordrecht, p. 1.
Schmidt D., 2002, Dynamo action of magnetostrophics waves. In: *Advances in Nonlinear Dynamos*.
Schmidt W., Hofmann A., Balthasar H., Tarbell T.D., Frank Z.A., 1992, *Astron. Astrophys.* **264**, L27.
Schmieder B., del Toro Iniesta J.C., Vázquez M. (Eds.), 1997, *Advances in the Physics of Sunspots*, ASP Conf. Ser. Vol. 118.
Schou J., Christensen-Dalgaard J., and Thompson M.J., 1992, *Astrophys. J.* **385**, L59.
Schou J., Antia H.M., Basu S., 1998, *Astrophys. J.* **505**, 390.
Schou J., Howe R., Basu S., et al., 2002, *Astrophys. J.* **567**, 1234.
Schrijver C.J., Title A.M., Harvey K.L., et al., 1998, *Nature* **394**, 152.
Schrijver C.J., Title A.M., Berger T.E., et al., 1999, *Sol. Phys.* **187**, 261.
Schüssler M., 1979, *Astron. Astrophys.* **71**, 79.
Schüssler M., Caligari P., Ferriz-Mas A., Moreno-Insertis F., 1994, *Astron. Astrophys.* **281**, L69.
Schüssler M., Shelyag S., Berdyugina S., Vögler A., Solanki S.K., 2003, *Astrophys. J.* **597**, L173.
Schwenn R., 1990, Large-scale structure of the interplanetary medium. In: *Physics of the Inner Heliosphere*, Vol. I, Schwenn R., Marsch E. (Eds), Springer, Berlin, p. 99.
Schwenn R., 1993, Interplanetary plasma and magnetic field (solar wind), In: *Landolt-Börnstein Astronomy and Astrophysics New Series VI/3a*

'Instruments, Methods, Solar System', H.H. Voigt (Ed.), Springer, Berlin, Chap. 3.3.5.2, p. 189.

Shelyag S., Schüssler M., Solanki S.K., Berdyugina S., Vögler A., 2004, *Astron. Astrophys.* submitted.

Sobotka M., 1997, in: *Advances in the Physics of Sunspots*, B. Schmieder et al. (Eds.), ASP Conf. Ser. Vol. 118, p. 155.

Socas Navarro H., Trujillo Bueno J., Ruiz Cobo R., 2000, *Science* **288**, 1396.

Solanki S.K., 1986, *Astron. Astrophys.* **168**, 311.

Solanki S.K., 1993, *Space Science Rev.* **63**, 1.

Solanki S.K., 2003, *Astron. Astrophys. Rev.* **11**, 153.

Solanki S.K. and Montavon C.A.P., 1993, *Astron. Astrophys.* **275**, 283.

Solanki S.K. and Rüedi I., 2003, *Astron. Astrophys.* **411**, 249.

Solanki S.K. and Steiner O., 1990, *Astron. Astrophys.* **234**, 519.

Solanki S.K., Lagg A., Woch J., Krupp N., Collados M., 2003, *Nature* **425**, 692.

Spruit H.C., 1976, *Sol. Phys.* **50**, 269.

Stein R.F. and Nordlund Å, 2002, in *SOLMAG 2002: Proc. Magnetic Coupling of the Solar Atmosphere*, Euroconference and IAU Colloquium 188, H. Sawaya-Lacoste (Ed.), ESA SP-505, p.83.

Steiner O., Pneuman G.W., Stenflo J.O., 1986, *Astron. Astrophys.* **170**, 126.

Steiner O., Grossmann-Doerth U., Knölker M., Schüssler M., 1998, *Astrophys. J.* **495**, 468.

Stenflo J.O., 1973, *Sol. Phys.* **32**, 41.

Stenflo J.O., 1994, *Solar Magnetic Fields: Polarized Radiation Diagnostics*, Kluwer, Dordrecht.

Stucki K., Solanki S.K., Pike C.D., et al., 2002, *Astron. Astrophys.* **381**, 653.

Thomas J.H., Weiss N.O. (Eds.), 1992, *Sunspots: Theory and Observations*, Kluwer, Dordrecht.

Thompson M.J., Christensen-Dalsgaard J., Miesch M.S., Toomre J., 2003, *Ann. Rev. Astron. Astrophys.* **41**, 599.

Title A.M., Frank Z.A., Shine R.A., et al., 1993, *Astrophys. J.* **403**, 780.

Tomczyk S., Schou J., and Thompson M.J., 1995, *Astrophys. J.* **448** L57.

Unruh Y.C., Solanki S.K., Fligge M., 1999, *Astron. Astrophys.* **345**, 635.

Vögler A., 2003, PhD Thesis, Univ. Göttingen.

Vögler A. and Schüssler M., 2003, *Astron. Nachr.* **324**, 399.

Walton S.R., Premiger D.G., Chapman G.A., 2003, *Astrophys. J.* **590**, 1088.

Webb, D., 2000, Coronal Mass Ejections: Origins, Evolution, and Role. In: *Space Weather*, IEEE Transactions on Plasma Science, Vol. 28, 1795.

Weber E.J., Davis L., Jr., 1967, *Astrophys. J.* **148**, 217.

Westendrop Plaza C., del Toro Iniesta J.C., Ruiz Cobo B., Martínez Pillet V., Lites B.W., Skumanich A., 1997, *Nature* **389**, 47.

White S.M., 2001, Observations of solar coronal magnetic fields. In: *Magnetic Fields Across the Herzsprung-Russel Diagram*, G. Mathys, S.K. Solanki, D.T. Wickramasinghe (Eds.), ASP Conf. Proc. Vol. 248, p. 67.

Winebarger A., Warren H.P., Mariska J.T., 2003, *Astrophys. J.* **587**, 439.

Woodard M.F. and Libbrecht K.G., 2003, *Sol. Phys.* **212**, 51.

Zayer I., Solanki S.K., Stenflo J.O., 1989, *Astron. Astrophys.*

Zhang J., Woch J., Solanki S.K., von Steiger R., 2002, *Geophys. Res. Lett.* **29**, 77.

Zwaan C. and Cram L.E., 1989, in *FGK Stars and T Tauri Stars*, L.E.. Cram, L.V. Kuhi (Eds.), NASA SP-502, p. 215.

Zwaan C. and Schrijver C.J., 2000, *Solar and Stellar Magnetic Activity*, Cambridge University Press.